

# Effect of Coconut Oil on the Properties of Thermoplastic Starch/Montmorillonite Nanoclay Bionanocomposite

Carlos Henrique Rodrigues Milfont<sup>a</sup> , Juciklécia da Silva Reinaldo<sup>b</sup> , Adriano Lincoln Albuquerque Mattos<sup>c</sup> ,  
Men de sa Moreira de Souza Filho<sup>c</sup> , Edson Noriyuki Ito<sup>d\*</sup> 

<sup>a</sup>Universidade Federal do Rio Grande do Norte, Programa de Pós-Graduação em Ciência e Engenharia de Materiais, Natal, RN, Brasil.

<sup>b</sup>Universidade do Estado do Amazonas, Escola Superior de Tecnologia, Manaus, AM, Brasil.

<sup>c</sup>Embrapa Agroindústria Tropical, Fortaleza, CE, Brasil.

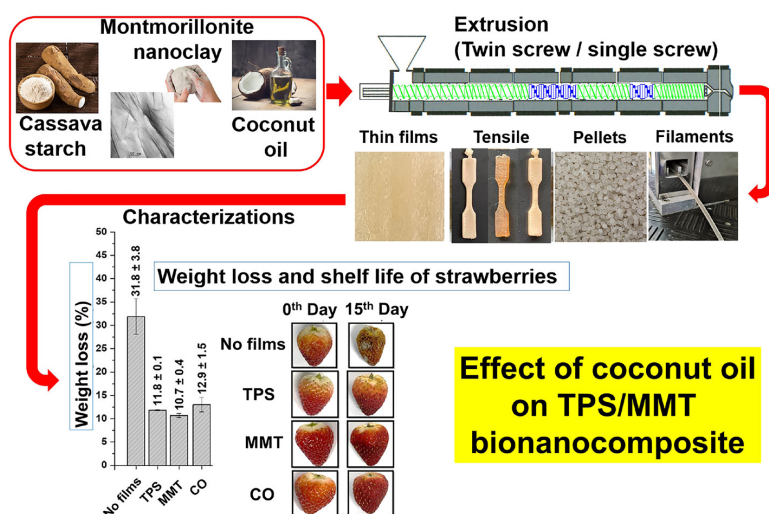
<sup>d</sup>Universidade Federal do Rio Grande do Norte, Departamento de Engenharia de Materiais, Natal, RN, Brasil.

Received: June 18, 2025; Revised: August 17, 2025; Accepted: September 21, 2025

This study aimed to develop cassava thermoplastic starch (TPS) biopolymers and polymer bionanocomposites with varying concentrations of montmorillonite (MMT) nanoclay and coconut oil (CO) by extrusion. X-ray diffraction indicated intercalated and partially exfoliated structure of nanoclay lamellae in the TPS, forming a polymer bionanocomposite. Colorimetric analyses showed that the color of the materials changed with variations in MMT and CO concentrations. The water absorption test revealed synergism between MMT and CO in reducing the hydrophilic character of the polymer bionanocomposite. Scanning electron microscopy (SEM) showed heterogeneities in the fracture surface morphologies of the biopolymer with CO droplets, absent in the TPS/MMT bionanocomposite. MMT addition destroyed CO droplets, favoring rougher and more uniform surfaces. Mechanical behavior under tensile test showed that MMT and CO improved these properties. TPS/MMT/CO bionanocomposites produced with sustainable materials showed potential for application in the production of films for packaging perishable fruits, such as strawberries, where the effect of reducing senescence and increasing the shelf life of the fruit was observed.

**Keywords:** Polymer bionanocomposite, thermoplastic starch, coconut oil, montmorillonite clay, extrusion.

## Visual abstract



\*e-mail: [edson.ito@ufrn.br](mailto:edson.ito@ufrn.br)

Associate Editor: Sandro Amico.

Editor-in-Chief: Luiz Antonio Pessan.

## 1. Introduction

Biodegradable polymers from natural renewable sources have been the focus of scientific and industrial interest for the development of new technologies that seek alternatives to replace synthetic plastics in short-lived applications. These polymers degrade quickly when discarded in the environment, reducing their environmental impact and enabling their use in packaging and other applications<sup>1-4</sup>.

Starch is an abundant polysaccharide in nature, inexpensive and can be obtained from different natural sources; therefore, it has been the focus of interest for the development of biodegradable materials<sup>5-9</sup>. Granular starch in its natural form does not have the characteristics of a thermoplastic polymer; however, processing starch at 90 to 180 °C and in the presence of a plasticizing agent, such as water or glycerol, transforms the starch into a biopolymer known as thermoplastic starch (TPS)<sup>10-14</sup>. TPS, as compared to synthetic polymers, has some limitations such as low mechanical and thermal resistance and high susceptibility to water absorption, which make it difficult to apply in most varied areas<sup>15-17</sup>. Studies<sup>18-24</sup> have been conducted to improve the limited properties of TPS by adding nanofillers and additives based on natural sources, such as montmorillonite (MMT) nanoclays and vegetable oils.

The use of MMT nanoclays in TPS matrices improves the mechanical and thermal properties of polymer nanocomposites because these inorganic fillers act as reinforcement at the nanometer scale, increasing the maximum strength, modulus of elasticity, and elongation at break, and improving the thermal stability of TPS<sup>18-22,24</sup>.

The use of vegetable oils, such as coconut oil (CO), has been used in research to improve the properties of TPS. The presence of oil with fatty acid chains in the starch structure improves the mechanical properties and reduces the hydrophilic nature of TPS<sup>19</sup>. Studies<sup>23-25</sup> have shown that the incorporation of low concentrations of CO into TPS reduces water absorption, improves the maximum strength, and inhibits microorganisms.

Research on the simultaneous addition of MMT nanoclays and vegetable oil to TPS<sup>26-31</sup> demonstrated that a synergistic effect exists between nanoclays and vegetable oils when incorporated into TPS matrices. Souza et al.<sup>29</sup> evaluated the effects of the combination of carvacrol essential oil and MMT nanoclay on the physicochemical properties of starch films. This study enabled the development of materials with good antimicrobial behavior, which was attributed to the intrinsic antimicrobial properties of the essential oil and MMT nanoclay ions, resulting in polymer bionanocomposites with excellent application potential in fresh foods such as fruits and vegetables.

Campos-Requena et al.<sup>30</sup> developed polymer bionanocomposites using TPS and MMT nanoclay containing extruded carvacrol and thymol essential oils. X-ray diffraction (XRD) and transmission electron microscopy (TEM) results showed that the polymer bionanocomposites exhibited a morphology with intercalated and exfoliated regions of nanoclay, resulting in an increase in the mechanical and thermal properties, as compared to pure TPS. The TPS nanocomposites exhibited application potential in active packaging with controlled release and antimicrobial properties resulting from the synergism of the interaction of the nanoclay with the essential oil.

Azevedo et al.<sup>31</sup> developed TPS/whey protein isolate/MMT bionanocomposites using extruded rosemary essential oil. The authors observed that the combination of low concentrations of rosemary essential oil and MMT nanoclay in a TPS/whey protein-isolated bionanocomposite resulted in materials with improved thermal stability and barrier properties.

Previous studies<sup>26-31</sup> with TPS/MMT bionanocomposite using other vegetable oils demonstrated improvements in the final properties and potential for application in food packaging. Therefore, this study aimed to evaluate the effect of adding coconut oil on the physicochemical, optical, morphological, thermal, and mechanical properties of the cassava thermoplastic starch/MMT nanoclays bionanocomposite and its applicability as bioactive packaging.

## 2. Materials and Methods

### 2.1. Materials

Commercial cassava starch was acquired from Yoki Alimentos S/A (18% amylose), PA glycerol (99.5% purity) was acquired from Dinâmica Contemporânea Ltd., distilled water, coconut oil (CO) was acquired from Copra Industria Alimentícia Ltda., and montmorillonite (MMT) nanoclay Cloisite 30B was acquired from Southern Clays. All plant-based materials used in this study had already been registered in the Brazilian Government Genetic Patrimony System and Associated Traditional Knowledge (SisGen), Access Register No. A6BF998.

### 2.2. Preparation of materials

#### 2.2.1. Pre-mixing of components

All components were initially weighed on an analytical scale, where the proportions of starch, glycerol, and water were based on the study by Reinaldo et al.<sup>32</sup>. Table 1 lists the proportions of each component.

Pre-mixing was performed using a 400 W internal mixer at its calculated maximum speed was around 400 rpm for 10 min. The nanoclays in the formulations were first dispersed in distilled water using a mechanical stirrer (MA147, Marconi Equipamentos Ltda.) at 500 W and a stirring speed of 500 rpm

**Table 1.** Proportion of the components in the mixtures.

| Formulation                      | Mixture Code | Composition (phr) |
|----------------------------------|--------------|-------------------|
| Starch/Glycerol/Water            | TPS          | 100/45/15         |
| Starch/Glycerol/<br>Water/MMT    | 1MMT         | 100/45/15/1       |
|                                  | 3MMT         | 100/45/15/3       |
| Starch/Glycerol/Water/CO         | 1CO          | 100/45/15/1       |
| Starch/Glycerol/<br>Water/MMT/CO | 1MMT/1CO     | 100/45/15/1/1     |
|                                  | 3MMT/1CO     | 100/45/15/3/1     |
| Starch/Glycerol/Water/CO         | 5CO          | 100/45/15/5       |
| Starch/Glycerol/<br>Water/MMT/CO | 1MMT/5CO     | 100/45/15/1/5     |
|                                  | 3MMT/5CO     | 100/45/15/3/5     |
| Starch/Glycerol/Water/CO         | 10CO         | 100/45/15/10      |
| Starch/Glycerol/<br>Water/MMT/CO | 1MMT/10CO    | 100/45/15/1/10    |
|                                  | 3MMT/10CO    | 100/45/15/3/10    |

for 1 h before being mixed with starch. The mixtures were placed in plastic bags, hermetically sealed, identified, and conditioned in a freezer at approximately 4 °C for 24 h.

### 2.2.2. Extrusion processing

The mixtures were processed using a co-rotational twin screw extruder (AX Plásticos Máquinas Técnicas Ltda.) with a diameter of 16 mm and l/d of 40, which was used to prepare pure TPS, TPS with CO, and polymer nanocomposites under the same conditions, that is, with a temperature profile of 50/60/110/110/120/125/130/130/135 °C from feed to die, a screw speed of 180 rpm, and hopper feed of 30 rpm using a die for pellet production.

After the extrusion mixing of the polymer bionanocomposites, test specimens (ASTM D638<sup>33</sup> Type V) were produced using injection molding. This process was carried out with a Thermo Scientific HAAKE MiniJet II injection molding system, operating at a gun temperature of 130 °C, an injection pressure of 550 bar, and a mold temperature of 40 °C. The specimens were conditioned at 23 °C and 50% relative humidity (RH) before analysis.

## 2.3. Characterization of polymer bionanocomposites

### 2.3.1. X-ray diffraction

The X-ray diffraction patterns were obtained in a Shimadzu diffractometer, model XRD-7000, using CuK $\alpha$  radiation ( $\lambda = 1.5418 \text{ \AA}$ ) at 40 kV and 30 mA, at a speed of 1° (2 $\theta$ )/min with a step of 0.05. The tests were carried out at room temperature and in the range of 2 $\theta$  angles from 2.5 to 60°.

### 2.3.2. Water absorption

Water absorption tests were conducted in accordance with ASTM D570<sup>34</sup>, using rectangular specimens cut from the injection-molded samples. The materials were initially dried in a vacuum oven at 50 °C for 24 h and then the samples were weighed on an analytical scale and immersed in distilled water at 23 °C. These samples were weighed at 20 min intervals up to maximum of 6 h. Water absorption was measured using Equation 1:

$$\text{Water absorption(\%)} = \left( \frac{M_1 - M_0}{M_0} \right) \times 100 \quad (1)$$

where M1 is the mass of the sample (g) after immersion in water and M0 is the mass of the sample before immersion in water.

### 2.3.3. Color parameters and visual appearance

The L\*, a\*, and b\* parameter values of them were measured using a colorimeter (CM-5, Konica Minolta). Measurements were performed thrice on a white background and the average of at least three measurements on each surface was reported. Equation 2 was used to determine the total color difference caused by the introduction of CO and clay into the TPS matrix using the L\*, a\*, and b\* parameters:

$$\Delta E^* = \sqrt{(\Delta L^*)^2 + (\Delta a^*)^2 + (\Delta b^*)^2} \quad (2)$$

where  $\Delta E^*$  is the color difference,  $\Delta L^* = L_{\text{TPS}}^* - L_{\text{Formulation}}^*$ ,  $\Delta a^* = a_{\text{TPS}}^* - a_{\text{Formulation}}^*$ , and,  $\Delta b^* = b_{\text{TPS}}^* - b_{\text{Formulation}}^*$

### 2.3.4. Morphological characterization

The samples were cryofractured at -18 °C before analysis and this surface was coated with a thin conductive layer of gold. Morphological analyses of the fracture surfaces of the TPS, TPS/CO and polymer nanocomposites with and without CO were performed using scanning electron microscopy (SEM; Zeiss Auriga 40) with a field-emission gun (with a tungsten filament).

### 2.3.5. Thermal characterization

Thermogravimetric analyses (TGA) of samples were performed from ambient temperature to 400 °C at 10 °C min<sup>-1</sup> using a Perkin Elmer STA 6000 simultaneous thermal analyzer under a nitrogen atmosphere with a flow rate of 40 mL min<sup>-1</sup>.

### 2.3.6. Mechanical characterization

Tensile tests were conducted using an EMIC DL-3000 universal testing machine, equipped with a 500 N load cell. The tests followed ASTM D638<sup>33</sup> Type V specifications, displacement rate was 10 mm min<sup>-1</sup>.

### 2.3.7. Performance of the films as packaging for strawberries

Initially, thin films with a thickness of 1 mm were obtained from the materials granules in an EMIC press at a temperature of 160 °C, a plasticization time of 5 min, with a pressing time of 2 min and a load of 40 N. The performances of the films as packaging materials for strawberries were evaluated according to the methodology described by Ferreira et al.<sup>13</sup>. Strawberries (*Fragaria ananassa*) were purchased from a local market (Natal-RN, Brazil), washed in water, dipped in a sodium hypochlorite solution (250 ppm), and dried at room temperature. Fruits without imperfections, deep marks, or signs of rotting were selected, weighed, and placed in an acrylic box that was sealed with different films. Strawberries with and without the films (control) were stored in a refrigerator at 4 °C  $\pm$  1 °C for a period of 15 d. The strawberries (in triplicate) were weighed daily, and the mass loss was expressed as the percentage of mass loss, which was calculated using Equation 3:

$$WL(\%) = \left( \frac{W_0 - W_t}{W_0} \right) \times 100 \quad (3)$$

where W0 is the initial weight of the strawberry and Wt is the weight of the strawberry at time t (in days).

## 2.4. Statistical analyses

Statistical analyses were conducted using Statistica 12 software (StatSoft Inc.). A one-way analysis of variance (ANOVA) was employed to evaluate the results, followed by Tukey's post hoc test to determine significant differences, with a significance level set at  $p < 0.05$ . Data were presented as the mean  $\pm$  standard deviation (SD) based on at least sextuplicate measurements.

## 3. Results and Discussion

### 3.1. X-ray diffraction

Figure 1 shows the X-ray diffractograms for granular starch, MMT, TPS, the biopolymer with CO, and the polymer

bionanocomposite. Native starches generally exhibit crystallinity owing to the organization of amylopectin molecules inside the granules. Cassava starch exhibited characteristic diffraction peaks at  $2\theta = 15.02^\circ$ ,  $17.45^\circ$ , and  $23.01^\circ$ , with corresponding interplanar distances of 0.58 nm, 0.51 nm, and 0.38 nm, respectively. These values are similar to those reported by Singh et al.<sup>35</sup> and Sun et al.<sup>36</sup>, indicating that the cassava starch granules used in this study exhibited A-type crystallinity, a monoclinic structure characteristic of cassava starch. The crystallinity index (CI) was calculated to be 17.6%, which further supports the presence of crystallinity in the cassava starch.

The peaks exhibited by the extruded TPS differed from those observed for granular starch, indicating that the semi-crystalline structure of the granules was destroyed during mixing. The extruded TPS exhibited a crystallinity of 13.2%. The diffraction peaks typically associated with starch crystallinity, often observed in thermoplastic starch, at  $2\theta = 13^\circ$ ,  $18^\circ$ , and  $20^\circ$  were not clearly visible in the TPS pattern, which was instead dominated by a broad amorphous halo. Such peaks, when present, may arise from recrystallization of amylose chains during post-processing cooling or during storage of the processed material.

The TPS/CO biopolymer (in regions B and C of Figure 1) exhibited peaks at approximately  $13^\circ$ ,  $19^\circ$ , and  $20^\circ$ , similar to those observed in the TPS diffractogram but with greater intensity. The incorporation of coconut oil (CO) influenced the crystalline structure of TPS, although the crystallinity index (CI) values of the formulations containing CO, suggest a slight reduction in overall crystallinity compared to pure TPS (CI = 13.2%). Specifically, formulations such as 1CO (10.5%), 5CO (12.1%), and 10CO (10.9%) exhibited lower CI values, indicating that although CO may promote some degree of recrystallization through the formation of amylose-lipid complexes (V-type crystalline structures), the net effect is a reduction in long-range molecular order due to the plasticizing of CO. These results corroborate those obtained by Ployetchara and Gohtani<sup>37</sup> and Wang et al.<sup>38</sup>, which report the capacity of lipids to interact with amylose chains.

The nanoclay in the TPS/MMT bionanocomposite favored the recrystallization of starch with the formation of a V-type crystalline structure, as observed by the increase in the intensity of the characteristic peaks ( $2\theta = 13^\circ$ ,  $17^\circ$ , and  $20^\circ$ ) referring to this crystalline structure at 3MMT. Region A in Figure 1 shows that the main characteristic peak of MMT clay was at approximately  $2\theta = 4.94^\circ$ , corresponding to an interplanar distance ( $d_{001}$ ) of 1.8 nm, which is similar to that reported by Derungs et al.<sup>39</sup>. The 1 and 3 wt.% MMT compositions did not exhibit peaks at  $2\theta = 4.94^\circ$ , indicating the possible formation of a TPS/MMT bionanocomposite with a possible intercalated and partially exfoliated structure. Previous studies<sup>40</sup> have reported that the disappearance of the clay characteristic peak is an indication of an increase in the basal spacing between the silicate lamellae resulting from intercalation with the polymeric chains of the cassava starch in the nanoclay lamellae and from its complete exfoliation, which leads to the formation of polymer bionanocomposites. These results indicate the intercalation and partial exfoliation and development of TPS/MMT bionanocomposites owing to the premixing strategy of nanoclay/water dispersion in TPS and further processing with a high shear rate.

The TPS/MMT/CO bionanocomposite exhibited a behavior similar to that of the TPS/MMT bionanocomposite, with the disappearance of the peak related to MMT, suggesting the maintenance of intercalated or exfoliated structures. These formulations exhibited peaks related to the V-type crystalline structure that were more intense in the formulations containing 3 wt.% MMT and moderate to high concentrations of CO, particularly in the 3MMT/5CO formulation, which exhibited the highest crystallinity index among all samples (17.5%). As observed by other researchers<sup>41,42</sup>, the organically modified nanoclay interacted effectively with the TPS matrix and CO owing to the presence of hydroxyl groups (-OH), which promoted greater interaction, allowing the formation of a disorganized structure or partial exfoliation, indicating that there was synergism of the components in the formation of these materials.

### 3.2. Water absorption

Figure 2 shows the water absorption curves, while Table 2 presents the water absorption values after 360 minutes of immersion for pure TPS, TPS/CO, TPS/MMT, and TPS/MMT/CO with varying concentrations of MMT

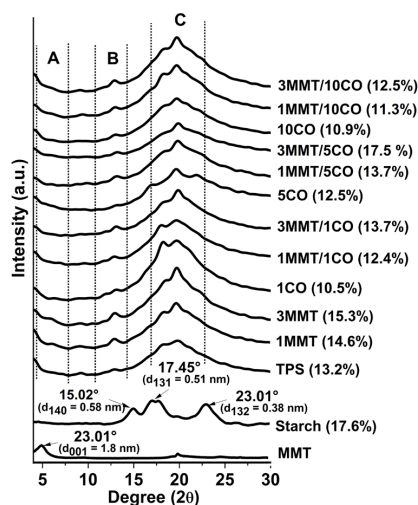


**Figure 1.** XRD diffractograms of MMT, starch, TPS, TPS/CO, TPS/MMT, and TPS/MMT/CO.

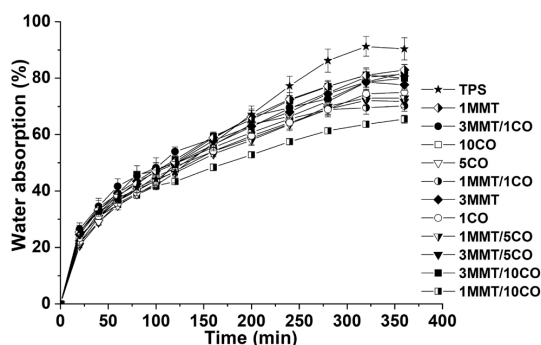


**Figure 2.** Water absorption versus time curves for pure TPS, TPS/CO, TPS/MMT, and TPS/MMT/CO.



**Table 2.** Water absorption after 360 minutes for pure TPS, TPS/CO, TPS/MMT, and TPS/MMT/CO.

| Formulation | Water absorption (%) |
|-------------|----------------------|
| TPS         | 90.4 ± 3.9g          |
| 1MMT        | 82.8 ± 1.9b          |
| 3MMT        | 77.6 ± 1.8ac         |
| 1CO         | 75.0 ± 2.4de         |
| 1MMT/1CO    | 80.2 ± 3.5ab         |
| 3MMT/1CO    | 81.8 ± 3.0ab         |
| 5CO         | 80.0 ± 2.2ab         |
| 1MMT/5CO    | 72.9 ± 2.2cde        |
| 3MMT/5CO    | 71.7 ± 2.1cd         |
| 10CO        | 81.4 ± 1.3ab         |
| 1MMT/10CO   | 65.4 ± 1.4f          |
| 3MMT/10CO   | 70.1 ± 1.8c          |

Different letters indicate a significant difference according to the Tukey HSD test ( $p < 0.05$ ), one-way factor

and CO as a function of time. TPS exhibited a higher water absorption at 360 min ( $90.4 \pm 3.9\%$ ) due to its low crystallinity, as observed in the XRD analysis, along with its inherent hydrophilic character. Both native starch and the plasticizer (glycerol) used to obtain thermoplastic material are hydrophilic, which further contributes to the increased water absorption. The addition of up to 5 wt.% CO to TPS promoted a reduction in water absorption. Similar results were reported by Iamareerat et al.<sup>27</sup> and Bhasney et al.<sup>43</sup>, indicating that the reduction in the water absorption curves may have occurred because of the hydrophobic nature of CO, which reduced the presence of hydrophilic regions in the TPS and consequently reduced the possibility of hydrogen bonding of the macromolecules present in the starch with water molecules, hindering their diffusion into the interior of the materials. Qian et al.<sup>44</sup> and Monteiro et al.<sup>45</sup> stated that this reduction may also be associated with the formation of the amylose-lipid complexes observed in the XRD results because the increase in crystallinity hinders the diffusion of water molecules into the material.

The TPS/MMT bionanocomposites with 1 and 3 wt.% nanoclay (1MMT and 3MMT) showed a reduction in the water absorption curve at 360 min, as compared with TPS, with water absorption values of  $82.8 \pm 1.9\%$  and  $77.6 \pm 1.8\%$ , respectively. Aouada et al.<sup>46</sup> reported that the reduction in water absorption may be due to the good interaction of the nanoclay lamellae with the TPS matrix formed by hydrogen bonding-type bonds that hinder the diffusion of water molecules into the interior of the material. The formation of intercalated and partially exfoliated structure regions in the 1MMT and 3MMT bionanocomposite matrices, as observed in the XRD results, may reduce water absorption in these compositions. TPS/MMT/CO bionanocomposites containing 5 wt.% or more of CO exhibited an even more pronounced reduction in water absorption over time. The 3MMT/10CO formulation, for example, presented a crystallinity index of 12.5% and a water absorption of  $70.1 \pm 1.8\%$  at 360 minutes, indicating a significant enhancement in water resistance. This improvement is likely due to the synergistic effect between the hydrophobic CO and the partially exfoliated nanoclay layers, which reduce the hydrophilic character of TPS and

its interaction with water molecules, resulting in materials with improved moisture resistance.

### 3.3. Color parameters

Table 3 list the color parameters  $L^*$ ,  $a^*$ ,  $b^*$ , the color variation ( $\Delta E^*$ ), and the visual appearance of TPS, TPS/CO, and the polymer bionanocomposite. The results showed that pure TPS had luminosity  $L^*$ ,  $a^*$ , and  $b^*$  parameter values of 35.51, 1.65, and 5.61, respectively, with a translucent appearance and yellow hue. The color, appearance, and opacity parameters changed because of variations in the concentrations of MMT and CO in the TPS matrix.

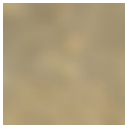


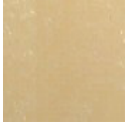




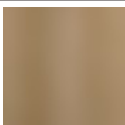
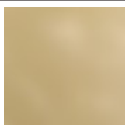
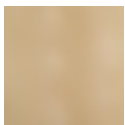

The presence of CO in the TPS increased the  $L^*$  parameter value of the TPS biopolymer, increasing the luminosity of the material. This increase in the  $L^*$  parameter value was more pronounced for the formulation with 1 wt.% CO, which exhibited a more luminous appearance and a light hue, which was attributed to the formation of an emulsion during extrusion that corroborated the formation of CO droplets distributed along the TPS matrix, as seen in the SEM photomicrographs in Figure 3. Chantrapornchai et al.<sup>47</sup> stated that the formation of lipid droplets in a material tends to favor the scattering of incident light in the sample, causing an increase in the material luminosity and color variation of these materials. The  $a^*$  and  $b^*$  parameter values of the TPS/CO biopolymer decreased with an increasing CO concentration, indicating a tendency towards a light yellow and shiny color for the 1 wt.% CO composition and a dark yellow and opaque color for the 5 and 10 wt.% CO compositions.

The presence of 1 and 3 wt.% MMT nanoclay in the polymer bionanocomposite reduced the  $L^*$  parameter of the material to 34.76 and 34.59, respectively. The polymer bionanocomposites exhibited significant color variation, as compared to pure TPS. The polymer bionanocomposites exhibited brown colors with light and dark tones, and the TPS composition with 3 wt.% MMT exhibited a significant increase in the  $a^*$  parameter value. The color changes to the presence of metallic ions, such as  $Fe^{2+}$  and  $Fe^{3+}$ , in the nanoclay and/or cation exchanges occurring during extrusion that alter the color of the polymer nanocomposites, which resulted in a darker color for these formulations.

The TPS/MMT bionanocomposite with 1 wt.% CO exhibited a slight increase in the  $L^*$  and  $a^*$  parameter values and a light brown hue. However, the increase in MMT concentration promoted a reduction in the color parameters and coloration of the 3MMT/1CO bionanocomposite, which was more pronounced in the  $b^*$  parameter value, exhibiting a more intense brown color than the 1MMT/1CO bionanocomposite.

The TPS/MMT nanocomposites with high concentrations of CO exhibited a considerable increase in the  $L^*$  parameter value, particularly for the bionanocomposite with 3 wt.% MMT. This occurred because of the absence of CO droplets in the TPS bionanocomposite matrix due to the addition of MMT, which spread the CO in the TPS matrix for the composition with 5 wt.% CO. The excess CO in the bionanocomposite with 10 wt.% CO migrated to the surface, which further favored the scattering of incident light and consequently increased the surface brightness of the material.

**Table 3.** Color parameters and visual aspect of TPS, TPS/CO, TPS/MMT, and TPS/MMT/CO.

|                  | <i>L</i> *      | <i>a</i> *   | <i>b</i> *     | $\Delta E^*$  | <i>Visual Aspect</i>  |
|------------------|-----------------|--------------|----------------|---------------|---|
| <i>TPS</i>       | 35.51 ± 0.80ab  | 1.65 ± 0.16a | 5.61 ± 0.54b   | -             |    |
| <i>1MMT</i>      | 34.76 ± 0.89a   | 1.63 ± 0.40a | 4.55 ± 0.69abc | 1.84 ± 0.48a  |    |
| <i>3MMT</i>      | 34.59 ± 1.17a   | 1.85 ± 0.20a | 5.11 ± 1.01ab  | 1.82 ± 0.92a  |    |
| <i>1CO</i>       | 38.29 ± 0.90bc  | 1.54 ± 0.17a | 5.06 ± 0.69ab  | 2.89 ± 0.47a  |    |
| <i>1MMT/1CO</i>  | 38.9 ± 0.77c    | 1.68 ± 0.16a | 5.05 ± 0.18ab  | 3.49 ± 0.33a  |    |
| <i>3MMT/1CO</i>  | 35.81 ± 0.56ab  | 1.10 ± 0.42a | 2.74 ± 0.55c   | 2.95 ± 1.01a  |   |
| <i>5CO</i>       | 36.00 ± 0.66ab  | 1.03 ± 0.12a | 4.11 ± 0.28abc | 1.86 ± 0.80a  |  |
| <i>1MMT/5CO</i>  | 39.66 ± 1.15c   | 0.97 ± 0.21a | 4.23 ± 0.59abc | 4.50 ± 1.74ab |  |
| <i>3MMT/5CO</i>  | 50.05 ± 0.78e   | 1.57 ± 0.22a | 7.55 ± 0.80d   | 14.71 ± 0.22c |  |
| <i>10CO</i>      | 36.82 ± 1.37abc | 0.78 ± 0.29a | 3.62 ± 0.78ac  | 2.91 ± 0.88a  |  |
| <i>1MMT/10CO</i> | 42.60 ± 0.33d   | 0.69 ± 0.11a | 3.45 ± 0.39ac  | 7.48 ± 0.83b  |  |
| <i>3MMT/10CO</i> | 56.70 ± 1.58f   | 1.90 ± 1.22a | 8.17 ± 0.41d   | 21.38 ± 2.32d |  |

Different letters in the same column indicate a significant difference according to the Tukey HSD test (p<0.05), one-way factor

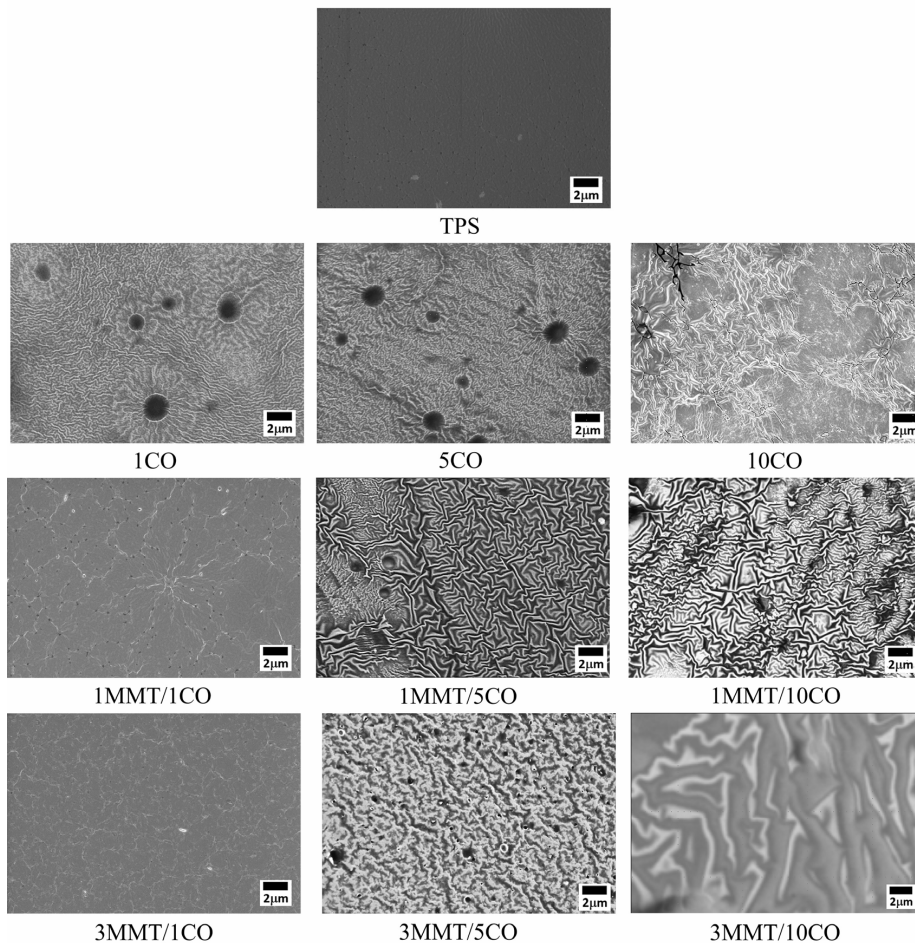


**Figure 3.** SEM photomicrographs of TPS, TPS/CO and TPS/MMT/CO with various MMT and CO concentrations.

The MMT spread or absorbed the CO droplets owing to the surfactant action of MMT, which led to an increase in the  $L^*$  parameter values, and the materials exhibited variations in color tones and a significant variation in  $\Delta E^*$ . The compositions containing 5 wt.% CO exhibited a color tendency to brown with a light hue with 1 wt.% MMT owing to a reduction in the  $a^*$  parameter value, and a dark hue owing to an increase in the MMT concentration, which favored an increase in the  $b^*$  parameter value. The composition with 10 wt.% CO and 1 and 3 wt.% MMT yielded light brown colors with light and glossy tones and a pearly gray color, respectively.

### 3.4. Scanning electron microscopy

Figure 3 shows SEM photomicrographs of the fracture surfaces of the TPS biopolymer and TPS/MMT bionanocomposites with various MMT and CO concentrations. All compositions containing CO exhibited heterogeneities. The addition of CO considerably altered the surface of the TPS matrix, and the samples exhibited different morphologies depending on the CO concentration. The TPS matrix in the biopolymers containing 1 and 5 wt.% CO exhibited a micellar-type morphology that may be associated with the formation of CO droplets owing to the immiscibility between TPS and CO.

The number of droplets scattered on the surface of the material at a CO concentration of 5 wt% increased, whereas an increase in the CO concentration significantly changed the morphology of the TPS, as observed in the photomicrograph of 10CO. The 10CO composition exhibited a rougher surface without the presence of miscella, which may be associated with the diffusion of lipid components to the material's surface during the extrusion process. The migration of these CO droplets to the surface of the material may have occurred as a result of excess CO, which may have favored coalescence, flocculation, and the creaming phenomenon. This occurs when lipid aggregates reach a critical size, at which point the density difference between the lipid and the continuous phase causes the formation of cream or the migration of lipid aggregates to the surface of the material. These results corroborate those presented in the literature on the incorporation of lipid components into TPS<sup>37,48,49</sup>.

The incorporation of CO into the TPS/MMT bionanocomposite altered their fracture surface morphologies. These fracture surfaces were examined and compared with those of the TPS/CO biopolymer in the same concentrations. The bionanocomposite with 1 wt% of MMT and 1 wt% of CO (1MMT/1CO) exhibited a fracture surface with smoother regions and the presence of CO droplets with smaller sizes

and uniform distribution in the TPS matrix, as compared with the fracture surfaces of the TPS biopolymer with 1 wt% CO. Increasing the concentration of MMT in the TPS/MMT/CO bionanocomposite with 3 wt% of MMT and 1 wt% of CO (3MMT/1CO) to 3 wt.% resulted in the formation of a more homogeneous and smoother surface with the presence of few droplets of CO smaller than those observed in the 1MMT/1CO composition.

The TPS/MMT bionanocomposites with 5 and 10 wt.% CO exhibited rougher surfaces than those of the bionanocomposites with 1 wt.% CO (1MMT/1CO and 3MMT/1CO). This roughness suggests that the spreading of CO on the surface of the bionanocomposite was due to the presence of clay. The 3MMT/10CO composition exhibited a surface with smooth regions and little roughness without the presence of CO in the TPS matrix. This may have occurred because of the excess CO in this composition, which favored migration from the CO to the outer surface of the material. The observed results indicate that the organically modified MMT nanoclay may have acted as an oil retention agent, possibly owing to the presence of surfactants in the nanoclay, which may have favored the spread of CO in the TPS structure.

### 3.5. Thermogravimetric analysis

Figure 4 shows the thermogravimetric curves of the biopolymer and polymer bionanocomposites (TPS, TPS/CO, TPS/MMT, and TPS/MMT/CO), which shows that all compositions presented an initial mass loss at 80–150 °C that was associated with the loss of the surface moisture present in the materials.

The mass loss observed at 150–250 °C (Figure 4) in all samples was mainly associated with the loss of the glycerol present in the material. A greater loss of mass was observed in the formulations containing CO, which, according to Fangfang et al.<sup>23</sup> and Jayadas and Nair<sup>50</sup>, may be due to the thermal decomposition of CO, which involves the formation of volatile low-molar-mass hydrocarbons, carbon dioxide, and carbon monoxide.

A significant mass loss was observed at 250–400 °C (Figure 4), which is related to the maximum thermal decomposition rate of the materials. TPS exhibited the beginning of thermal degradation (Tonset) at 254 °C. These temperatures mainly indicate the thermal degradation of the amylose and amylopectin chains present in the starch. These results confirm previously reported findings on the thermal stability of TPS<sup>23,51,52</sup>. The TPS/MMT bionanocomposite showed a slight increase in Tonset compared to TPS, reaching 258 °C with the addition of 3 wt.% MMT, indicating that MMT can improve the thermal stability of the material. The TPS/MMT bionanocomposites containing CO exhibited the best thermal stability results, with a Tonset of 262 °C for the 3MMT/1CO and 261 °C for the 3MMT/5CO formulation. In all cases, the degradation temperature (Td) remained similar and close to 330 °C. The simultaneous addition of MMT and CO had a synergistic effect on the thermal stability of the polymer bionanocomposites. Chang et al.<sup>53</sup> reported that the strong interaction of the partial exfoliated clay lamellae with the TPS matrix, together with the V-type crystal structures observed in the XRD results, may have contributed to the increase in temperature, requiring higher levels of energy to initiate thermal degradation of the material.

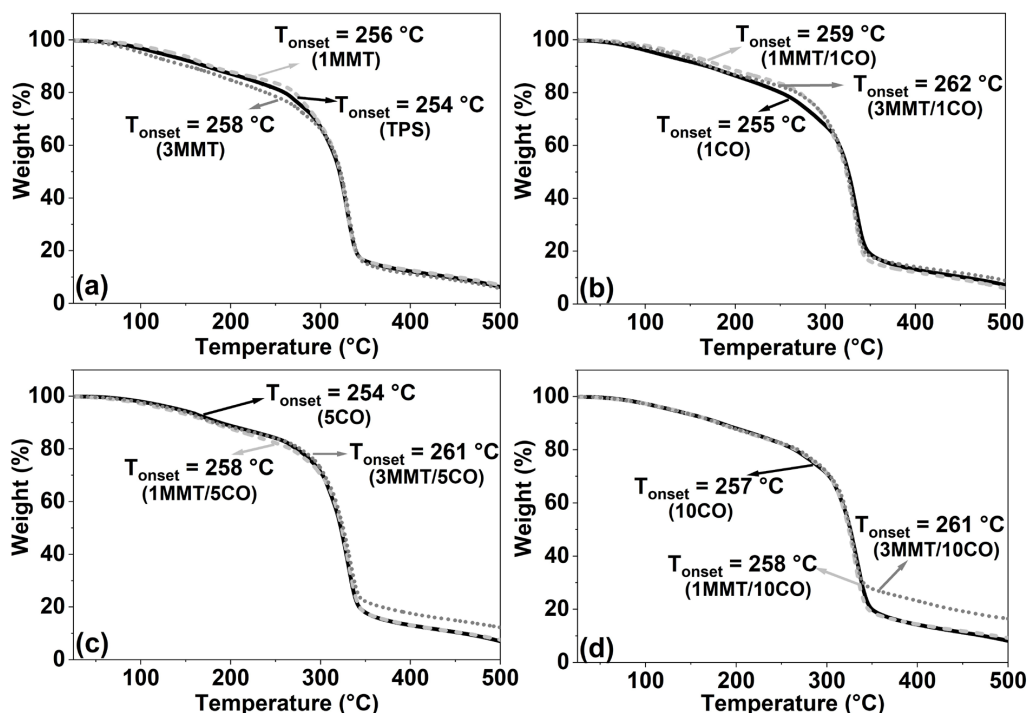


**Figure 4.** Thermogravimetric curves of the biopolymer and polymer bionanocomposites. (a) TPS, 1MMT, and 3MMT. (b) 1CO, 1MMT/1CO, and 3MMT/1CO. (c) 1MMT/5CO and 3MMT/5CO. (d) 10CO, 1MMT/10CO, and 3MMT/10CO.



### 3.6. Mechanical properties

Figure 5 shows stress-strain curves, while Table 4 summarizes the mechanical test results obtained from uniaxial tension tests on all injected samples. Pure TPS exhibited a maximum tensile strength of  $1.09 \pm 0.05$  MPa, an elongation at break of  $333 \pm 16\%$ , and an elastic modulus of  $1.52 \pm 0.39$  MPa, demonstrating limited mechanical performance. The addition of CO to the TPS/CO formulations slightly improved the tensile strength, with values ranging from 1.19 MPa to 1.29 MPa. Among these, the 5CO composition showed the highest strength ( $1.29 \pm 0.03$  MPa), indicating a slight reinforcement effect of CO on the TPS matrix.

The X-ray diffraction analysis revealed a reduction in the crystallinity index (CI) for CO-containing formulations, from 13.2% (TPS) to 10.5% (1CO), suggesting the presence of a more amorphous and flexible matrix. Nevertheless, a recrystallization process occurred, forming amylose-lipid complexes with a V-type crystalline structure, which contributed to the mechanical reinforcement observed, especially in formulations with moderate CO content. The incorporation of CO increased the elongation at break of the material, with the 10CO formulation reaching the highest value ( $460 \pm 14\%$ ), followed by 1MMT/10CO ( $363 \pm 16\%$ ) and 3MMT/10CO ( $315 \pm 18\%$ ). This behavior can be explained by the plasticizing effect of CO, which, being a liquid at room temperature, is dispersed as deformable droplets in the TPS matrix, as previously reported in SEM analyses. Studies<sup>49,54</sup> have shown that the presence of a heterogeneous structure with discontinuities owing to the presence of lipids in the TPS matrix can affect the mechanical properties. CO, which is a liquid at room temperature, is present in the material in the form of droplets, as observed in the SEM images, and can be easily deformed, increasing the elongation upon rupture of the material. These results corroborate those presented in the literature and the incorporation of lipid components into TPS<sup>55,56</sup>.

The addition of MMT significantly improved the mechanical strength and stiffness of the bionanocomposites. The 3MMT formulation exhibited the highest maximum tensile strength ( $3.92 \pm 0.14$  MPa) and elastic modulus ( $13.21 \pm 0.96$  MPa), correlated with the highest crystallinity index among all samples (15.7%). These improvements are

attributed to the reinforcing effect of the nanoclay and its ability to induce greater molecular organization within the TPS matrix. Ardakani et al.<sup>57</sup> reported that the good dispersion of the organically modified clay in the matrix contributes to an improvement in the mechanical properties of these materials under tension.

The combination of MMT and CO also contributed significantly to mechanical performance. The 3MMT/5CO formulation presented the highest tensile strength ( $4.75 \pm 0.15$  MPa), a high modulus ( $12.58 \pm 0.11$  MPa) and a CI of 17.5%, the highest observed in the study. These results confirm a synergistic effect between the nanoclay and the moderate presence of CO. However, formulations with 10 wt.% CO, even in the presence of MMT (1MMT/10CO and 3MMT/10CO), exhibited decreased mechanical performance, with reduced strength and modulus. This behavior reinforces that excessive CO content, beyond a certain limit, can act as a plasticizer in the TPS matrix, reducing maximum tensile strength and increasing elongation.

### 3.7. Performance of films as packaging for strawberries

To evaluate the potential use of the produced bionanocomposites as packaging, the extruded materials were thermoformed into films. Figure 6 shows the weight loss curve for strawberries without films (control) and those wrapped with films during 15 d of storage, while Figure 7 shows the visual appearance of

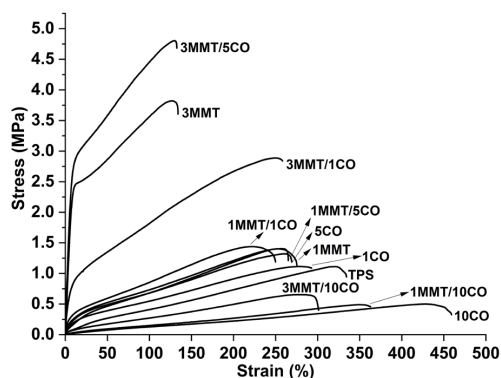


**Figure 5.** Stress versus strain curve for pure TPS, TPS/CO, TPS/MMT, and TPS/MMT/CO.

**Table 4.** Mechanical properties obtained from pure TPS, TPS/CO, TPS/MMT, and TPS/MMT/CO.

| Formulation | Maximum strength (MPa) | Elongation at break (%) | Modulus of elasticity (MPa) |
|-------------|------------------------|-------------------------|-----------------------------|
| TPS         | $1.09 \pm 0.05$ d      | $333 \pm 16$ ef         | $1.52 \pm 0.39$ ab          |
| 1MMT        | $1.48 \pm 0.07$ b      | $257 \pm 15$ ab         | $3.07 \pm 0.30$ cd          |
| 3MMT        | $3.92 \pm 0.14$ f      | $131 \pm 15$ c          | $13.21 \pm 0.96$ f          |
| 1CO         | $1.19 \pm 0.07$ ad     | $285 \pm 14$ bd         | $2.23 \pm 0.02$ bc          |
| 1MMT/1CO    | $1.42 \pm 0.03$ ab     | $248 \pm 7$ a           | $3.88 \pm 0.39$ d           |
| 3MMT/1CO    | $2.77 \pm 0.17$ e      | $257 \pm 13$ ab         | $6.39 \pm 0.27$ e           |
| 5CO         | $1.29 \pm 0.03$ abd    | $268 \pm 18$ ab         | $2.21 \pm 0.07$ bc          |
| 1MMT/5CO    | $1.41 \pm 0.02$ ab     | $270 \pm 10$ ab         | $5.24 \pm 0.04$ e           |
| 3MMT/5CO    | $4.75 \pm 0.15$ g      | $125 \pm 10$ c          | $12.58 \pm 0.11$ f          |
| 10CO        | $0.48 \pm 0.03$ c      | $460 \pm 14$ g          | $0.5 \pm 0.01$ a            |
| 1MMT/10CO   | $0.47 \pm 0.03$ c      | $363 \pm 16$ f          | $0.58 \pm 0.07$ a           |
| 3MMT/10CO   | $0.65 \pm 0.07$ c      | $315 \pm 18$ de         | $1.17 \pm 0.08$ a           |

Different letters in the same column indicate a significant difference according to the Tukey HSD test ( $p < 0.05$ ), one-way factor

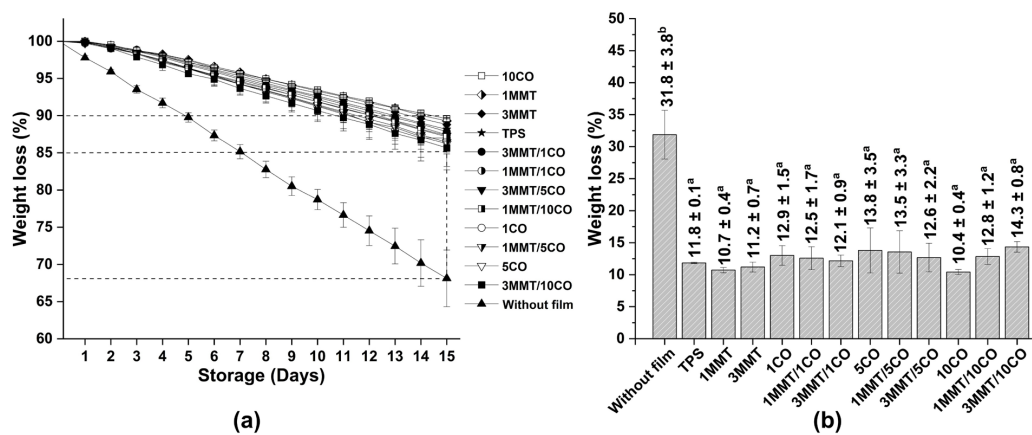


**Figure 6.** Weight loss of strawberries during refrigerated storage. (a) Daily weight loss curve of the strawberries. (b) Mass loss after 15 d of storage. For means, values that share a common letter are not significantly different (Tukey test,  $p < 0.05$ ).

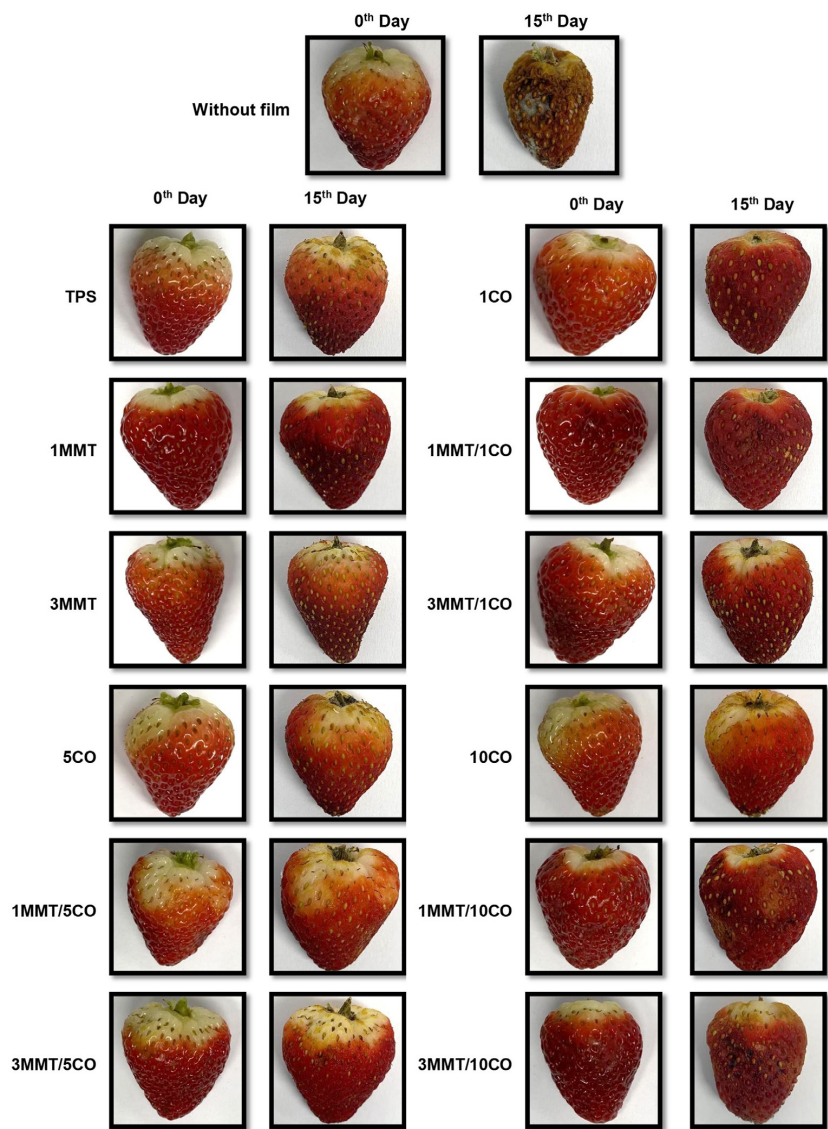


**Figure 7.** Effect of TPS, TPS/OC, TPS/MMT, and TPS/MMT/CO packaging on the quality and shelf life of strawberries after 15 d of storage in a refrigerated environment.

the strawberries at the beginning and end of the storage period (0 and 15 d, respectively). The results in Figure 6 show that the strawberries without films exhibited considerable mass loss over time, reaching  $31.8 \pm 3.8\%$  after 15 d. The post-test strawberries (15 d), as compared with the fresh strawberries (0 d), exhibited high shrinkage and dark spots, which were associated with fruit senescence. Similar results were reported by Rodrigues et al.<sup>58</sup> and can be attributed to the respiratory processes of fruits, loss of water and carbon to the external environment, and oxidative processes.

The strawberries packaged with TPS films, as compared with the unpackaged fruits, exhibited a reduction in weight loss of approximately 37% after 15 d as well as a visual improvement without the presence of dark spots or significant shrinkage. The post-testing strawberries (Figure 7), as compared with the fresh strawberries, exhibited a reddish color, opacity, and a small loss of brightness, which are associated with fruit dehydration over time. Studies<sup>55,59</sup> have shown that TPS films act as a physical barrier that partially blocks and hinders the diffusion of water, oxygen, and carbon dioxide molecules, thus increasing the shelf life of fruits.

The strawberries packaged with biopolymer and bionanocomposite films (Figure 6b) exhibited significantly lower mass loss compared to the unpackaged fruits, following a similar trend to those packaged with the TPS film. Among the samples, the bionanocomposites containing 1 and 3 wt.% of MMT showed a slightly reduced mass loss compared to the pure TPS film. This result is consistent with previous findings by Junqueira-Gonçalves et al.<sup>56</sup>, who reported that TPS-based bionanocomposites with clay lamellae dispersed in the polymer matrix can serve as physical barriers to the diffusion of water and gases. This barrier effect slows down the migration of water vapor, oxygen, and carbon dioxide between the interior of the fruit and the external environment.

The strawberries packaged with the 1MMT and 3MMT films also presented the best visual quality (Figure 7), maintaining a uniform color, surface brightness, and minimal signs of dehydration. These formulations presented crystallinity indices of 14.6% and 15.3%, respectively, values higher than that of neat TPS (13.2%), which may have contributed to their improved barrier performance. Additionally, similar mass loss values were observed in strawberries packaged with films containing 5 wt.% of coconut oil (CO), such as 5CO, 1MMT/5CO, and 3MMT/5CO. Notably, the 3MMT/5CO formulation exhibited the highest CI among all samples (17.5%). This increased crystallinity may have enhanced the molecular ordering and compactness of the polymer matrix, leading to reduced gas and moisture permeability. As a result, the packaging films based on 3MMT/5CO were likely more effective in preserving the freshness of strawberries during storage, despite not exhibiting the lowest numerical values of mass loss. These observations highlight the importance of considering multiple factors, including crystallinity, when evaluating the protective performance of packaging films.

## 4. Conclusions

A cassava TPS biopolymer containing CO and a TPS/MMT bionanocomposite with and without CO were obtained using the conventional extrusion mixing method. CO significantly improved the TPS biopolymer and TPS/MMT

bionanocomposite by reducing the hydrophilic character and improving the thermal and mechanical properties of the materials. This study indicates that the simultaneous incorporation of MMT clay and CO into bionanocomposites exhibits promising results for the physical and mechanical properties of these starch-based materials, expanding the possibility of using these sustainable materials in various industrial areas, such as packaging, contributing to reducing environmental impact and promoting eco-friendly practices.

## 5. Acknowledgements

The authors are grateful to the Coordination for the Improvement of Higher Education Personnel (CAPES) for the scholarship of Carlos Henrique Rodrigues Milfont (Project Number: 88887.373348/2019-00) in Graduate Program in Materials Science and Engineering of the Federal University of Rio Grande do Norte.

## 6. References

1. Tavanaie MA, Ghahari AH. A study on melt recycling of bio-based polypropylene/thermoplastic starch compound. *J Appl Polym Sci*. 2021;138(43):51282. <http://doi.org/10.1002/app.51282>.
2. Zhang S, He Y, Yin Y, Jiang G. Fabrication of innovative thermoplastic starch bio-elastomer to achieve high toughness poly(butylene succinate) composites. *Carbohydr Polym*. 2019;206:827-36. <http://doi.org/10.1016/j.carbpol.2018.11.036>.
3. Nguyen Vu HP, Lumdubwong N. Fabrication of starch blend films with different matrices and their mechanical properties. *Polym Test*. 2020;90:106694. <http://doi.org/10.1016/j.polymertesting.2020.106694>.
4. Rodriguez Llanos JH, Tadini CC, Gastaldi E. New strategies to fabricate starch/chitosan-based composites by extrusion. *J Food Eng*. 2021;290:110224. <http://doi.org/10.1016/j.jfoodeng.2020.110224>.
5. Gomez-Caturla J, Ivorra-Martinez J, Fenollar O, Balart R, Garcia-Garcia D, Dominici F, et al. Development of starch-rich thermoplastic polymers based on mango kernel flour and different plasticizers. *Int J Biol Macromol*. 2024;264:130773. <http://doi.org/10.1016/j.ijbiomac.2024.130773>.
6. Csiszár E, Nagy A, Fekete E. Contribution of flax-cellulose nanocrystals on the structural properties and performance of starch-based biocomposite films. *Express Polym Lett*. 2023;17(5):458-70. <http://doi.org/10.3144/expresspolymlett.2023.34>.
7. de Carvalho LGG, Marques NN, Fernandes RS, Villetti MA, Souza MSM Fo, Balaban RC. Effect of starch laurate addition on the properties of mango kernel starch films. *Mater Res*. 2021;24(3):e20200331. <http://doi.org/10.1590/1980-5373-mr-2020-0331>.
8. Chueangchayaphan W, Nooun P, Ummarat N, Chueangchayaphan N. Eco-friendly biocomposite foam from natural rubber latex and rice starch for sustainable packaging applications. *Express Polym Lett*. 2024;18(1):27-40. <http://doi.org/10.3144/expresspolymlett.2024.3>.
9. La Fuente CIA, do Val Siqueira L, Augusto PED, Tadini CC. Bio-based plastic based on ozonated cassava starch produced by extrusion. *J Polym Environ*. 2022;30(9):3974-84. <http://doi.org/10.1007/s10924-022-02488-0>.
10. Müller PS, Carpiné D, Yamashita F, Waszczynskij N. Influence of pinhão starch and natural extracts on the performance of thermoplastic cassava starch/PBAT extruded blown films as a technological approach for bio-based packaging material. *J Food Sci*. 2020;85(9):2832-42. <http://doi.org/10.1111/1750-3841.15355>.



11. da Silva JBA, Bretas RES, Lucas AA, Marini J, da Silva AB, Santana JS, et al. Rheological, mechanical, thermal, and morphological properties of blends poly(butylene adipate-co-terephthalate), thermoplastic starch, and cellulose nanoparticles. *Polym Eng Sci.* 2020;60(7):1482-93. <http://doi.org/10.1002/pen.25395>.
12. Montilla-Buitrago CE, Gómez-López RA, Solanilla-Duque JF, Serna-Cock L, Villada-Castillo HS. Effect of plasticizers on properties, retrogradation, and processing of extrusion-obtained thermoplastic starch: a review. *Stärke.* 2021;73(9-10):210060. <http://doi.org/10.1002/star.202100060>.
13. Ferreira RR, Souza AG, Quispe YM, Rosa DS. Essential oils loaded-chitosan nanocapsules incorporation in biodegradable starch films: a strategy to improve fruits shelf life. *Int J Biol Macromol.* 2021;188:628-38. <http://doi.org/10.1016/j.ijbiomac.2021.08.046>.
14. Dang KM, Yoksan R. Thermoplastic starch blown films with improved mechanical and barrier properties. *Int J Biol Macromol.* 2021;188:290-9. <http://doi.org/10.1016/j.ijbiomac.2021.08.027>.
15. Gomes ÁVR, Leite RHL, Silva MQ Jr, Santos FKG, Aroucha EMM. Influence of composition on mechanical properties of cassava starch, sisal fiber and carnauba wax biocomposites. *Materials Research.* 2019;22(suppl 1):e20180887.
16. Kumar Kesari A, Mulla AM, Razak SM, Munagala CK, Aniya V. Cellulose nanocrystals engineered TPS/PBAT granulation through extrusion process and application for compostable carry bags. *J Ind Eng Chem.* 2024;136:623-34. <http://doi.org/10.1016/j.jiec.2024.02.051>.
17. Weerapoprasit C, Prachayawarakorn J. Effects of polymethacrylamide-grafted branch on mechanical performances, hydrophilicity, and biodegradability of thermoplastic starch film. *Stärke.* 2019;71(11-12):1900068. <http://doi.org/10.1002/star.201900068>.
18. Staroszczyk H, Gottfried K, Malinowska-Pańczyk E, Kołodziejewska I. Clay-filled starch films. Part I: effect of clay kind and glycerol concentration on functional properties of composites. *Stärke.* 2017;69(1-2):1500325. <http://doi.org/10.1002/star.201500325>.
19. Schlemmer D, Angélica RS, Sales MJA. Morphological and thermomechanical characterization of thermoplastic starch/montmorillonite nanocomposites. *Compos Struct.* 2010;92(9):2066-70. <http://doi.org/10.1016/j.compstruct.2009.10.034>.
20. Saparová S, Ondříš L, Kovaříková M, Fričová O, Peidayesh H, Baran A, et al. Effects of glycerol content on structure and molecular motion in thermoplastic starch-based nanocomposites during long storage. *Int J Biol Macromol.* 2023;253:126911. <http://doi.org/10.1016/j.ijbiomac.2023.126911>.
21. Son D, Lee J, Kim SK, Hong J, Jung H, Shim JK, et al. Effect of cellulose nanofiber-montmorillonite hybrid filler on the melt blending of thermoplastic starch composites. *Int J Biol Macromol.* 2024;254:127236. <http://doi.org/10.1016/j.ijbiomac.2023.127236>.
22. Peidayesh H, Ahmadi Z, Khonakdar HA, Abdouss M, Chodák I. Fabrication and properties of thermoplastic starch/montmorillonite composite using dialdehyde starch as a crosslinker. *Polym Int.* 2020;69(3):317-27. <http://doi.org/10.1002/pi.5955>.
23. Fangfang Z, Xinpeng B, Wei G, Wang G, Shi Z, Jun C. Effects of virgin coconut oil on the physicochemical, morphological and antibacterial properties of potato starch-based biodegradable films. *Int J Food Sci Technol.* 2020;55(1):192-200. <http://doi.org/10.1111/ijfs.14262>.
24. Gutiérrez MC, del Carmen Nuñez-Santiago M, Romero-Bastida CA, Martínez-Bustos F. Effects of coconut oil concentration as a plasticizer and Yucca schidigera extract as a surfactant in the preparation of extruded corn starch films. *Stärke.* 2014;66(11-12):1079-88. <http://doi.org/10.1002/star.201400062>.
25. Xiao M, Tang B, Qin J, Wu K, Jiang F. Properties of film-forming emulsions and films based on corn starch/sodium alginate/gum Arabic as affected by virgin coconut oil content. *Food Packag Shelf Life.* 2022;32:100819. <http://doi.org/10.1016/j.fpsl.2022.100819>.
26. de Souza AG, dos Santos NMA, da Silva Torin RF, dos Santos Rosa D. Synergic antimicrobial properties of Carvacrol essential oil and montmorillonite in biodegradable starch films. *Int J Biol Macromol.* 2020;164:1737-47. <http://doi.org/10.1016/j.ijbiomac.2020.07.226>.
27. Iamareerat B, Singh M, Sadiq MB, Anal AK. Reinforced cassava starch based edible film incorporated with essential oil and sodium bentonite nanoclay as food packaging material. *J Food Sci Technol.* 2018;55(5):1953-9. <http://doi.org/10.1007/s13197-018-3100-7>.
28. Kashiri M, Maghsoudlou Y, Khomeiri M. Incorporating Zataria multiflora Boiss. essential oil and sodium bentonite nano-clay open a new perspective to use zein films as bioactive packaging materials. *Food Sci Technol Int.* 2017;23(7):582-96. <http://doi.org/10.1177/1082013217708526>.
29. Souza AC, Goto GEO, Mainardi JA, Coelho ACV, Tadini CC. Cassava starch composite films incorporated with cinnamon essential oil: antimicrobial activity, microstructure, mechanical and barrier properties. *Lebensm Wiss Technol.* 2013;54(2):346-52. <http://doi.org/10.1016/j.lwt.2013.06.017>.
30. Campos-Requena VH, Rivas BL, Pérez MA, Figueroa CR, Figueroa NE, Sanfuentes EA. Thermoplastic starch/clay nanocomposites loaded with essential oil constituents as packaging for strawberries – In vivo antimicrobial synergy over Botrytis cinerea. *Postharvest Biol Technol.* 2017;129:29-36. <http://doi.org/10.1016/j.postharvbio.2017.03.005>.
31. Azevedo VM, Carvalho RA, Borges SV, Claro PIC, Hasegawa FK, Yoshida MI, et al. Thermoplastic starch/whey protein isolate/rosemary essential oil nanocomposites obtained by extrusion process: antioxidant polymers. *J Appl Polym Sci.* 2019;136(23):47619. <http://doi.org/10.1002/app.47619>.
32. Reinaldo JS, Milfont CHR, Gomes FPC, Mattos ALA, Medeiros FGM, Lopes PFN, et al. Influence of grape and acerola residues on the antioxidant, physicochemical and mechanical properties of cassava starch biocomposites. *Polym Test.* 2021;93:107015. <http://doi.org/10.1016/j.polymertesting.2020.107015>.
33. ASTM: American Society for Testing and Materials. ASTM D638: standard test method for tensile properties of plastics. West Conshohocken: ASTM; 2022.
34. ASTM: American Society for Testing and Materials. ASTM D570: standard test method for water absorption of plastics. West Conshohocken: ASTM; 2022.
35. Singh V, Ali SZ, Somashekar R, Mukherjee PS. Nature of crystallinity in native and acid modified starches. *Int J Food Prop.* 2006;9(4):845-54. <http://doi.org/10.1080/10942910600698922>.
36. Sun J, He R, Gao F, Kou Z, Lan L, Lan P, et al. High-efficient preparation of cross-linked cassava starch by microwave-ultrasound-assisted and its physicochemical properties. *Stärke.* 2019;71(7-8):1800273. <http://doi.org/10.1002/star.201800273>.
37. Ployetchara T, Gohtani S. Effect of rice starch film blended with sugar (trehalose/allose) and oil (canola oil/coconut oil) on the physical properties and their interaction (Part II). *J Food Process Preserv.* 2021;45(10):e15795. <http://doi.org/10.1111/jfpp.15795>.
38. Wang L, Wang W, Wang Y, Xiong G, Mei X, Wu W, et al. Effects of fatty acid chain length on properties of potato starch–fatty acid complexes under partially gelatinization. *Int J Food Prop.* 2018;21(1):2121-34. <http://doi.org/10.1080/10942912.2018.1489842>.
39. Derungs I, Rico M, López J, Barral L, Montero B, Bouza R. Influence of the hydrophilicity of montmorillonite on structure and properties of thermoplastic wheat starch/montmorillonite bionanocomposites. *Polym Adv Technol.* 2021;32(11):4479-89. <http://doi.org/10.1002/pat.5450>.
40. Pirsas S, Mohtarami F, Kalantari S. Preparation of biodegradable composite starch/tragacanth gum/Nanoclay film and study of its physicochemical and mechanical properties. *Chem Rev Lett.* 2020;3(3):98-103.



41. Raquez J, Nabar Y, Narayan R, Dubois P. Preparation and characterization of maleated thermoplastic starch-based nanocomposites. *J Appl Polym Sci*. 2011;122(1):639-47. <http://doi.org/10.1002/app.30224>.
42. Müller CMO, Laurindo JB, Yamashita F. Composites of thermoplastic starch and nanoclays produced by extrusion and thermopressing. *Carbohydr Polym*. 2012;89(2):504-10. <http://doi.org/10.1016/j.carbpol.2012.03.035>.
43. Bhasney SM, Patwa R, Kumar A, Katiyar V. Plasticizing effect of coconut oil on morphological, mechanical, thermal, rheological, barrier, and optical properties of poly(lactic acid): a promising candidate for food packaging. *J Appl Polym Sci*. 2017;134(41):45390. <http://doi.org/10.1002/app.45390>.
44. Qian S, Sheng K, Yao W, Yu H. Poly(lactic acid) biocomposites reinforced with ultrafine bamboo-char: Morphology, mechanical, thermal, and water absorption properties. *J Appl Polym Sci*. 2016;133(20):app.43425. <http://doi.org/10.1002/app.43425>.
45. Monteiro MKS, Oliveira VRL, Santos FKG, Barros EL No, Leite RHL, Aroucha EMM, et al. Incorporation of bentonite clay in cassava starch films for the reduction of water vapor permeability. *Food Res Int*. 2018;105:637-44. <http://doi.org/10.1016/j.foodres.2017.11.030>.
46. Aouada FA, Mattoso LHC, Longo E. Enhanced bulk and superficial hydrophobicities of starch-based bionanocomposites by addition of clay. *Ind Crops Prod*. 2013;50:449-55. <http://doi.org/10.1016/j.indcrop.2013.07.058>.
47. Chantrapornchai W, Clydesdale F, McClements DJ. Influence of droplet characteristics on the optical properties of colored oil-in-water emulsions. *Colloids Surf A Physicochem Eng Asp*. 1999;155(2-3):373-82. [http://doi.org/10.1016/S0927-7757\(99\)00004-7](http://doi.org/10.1016/S0927-7757(99)00004-7).
48. Mohsenabadi N, Rajaei A, Tabatabaei M, Mohsenifar A. Physical and antimicrobial properties of starch-carboxy methyl cellulose film containing rosemary essential oils encapsulated in chitosan nanogel. *Int J Biol Macromol*. 2018;112:148-55. <http://doi.org/10.1016/j.ijbiomac.2018.01.034>.
49. Song X, Zuo G, Chen F. Effect of essential oil and surfactant on the physical and antimicrobial properties of corn and wheat starch films. *Int J Biol Macromol*. 2018;107:1302-9. <http://doi.org/10.1016/j.ijbiomac.2017.09.114>.
50. Jayadas NH, Nair KP. Coconut oil as base oil for industrial lubricants: evaluation and modification of thermal, oxidative and low temperature properties. *Tribol Int*. 2006;39(9):873-8. <http://doi.org/10.1016/j.triboint.2005.06.006>.
51. Katekhong W, Wongphan P, Klinmalai P, Harnkarnsujarit N. Thermoplastic starch blown films functionalized by plasticized nitrite blended with PBAT for superior oxygen barrier and active biodegradable meat packaging. *Food Chem*. 2022;374:131709. <http://doi.org/10.1016/j.foodchem.2021.131709>.
52. Trinh BM, Chang CC, Mekonnen TH. Facile fabrication of thermoplastic starch/poly (lactic acid) multilayer films with superior gas and moisture barrier properties. *Polymer*. 2021;223:123679. <http://doi.org/10.1016/j.polymer.2021.123679>.
53. Chang F, He X, Fu X, Huang Q, Jane J. Effects of heat treatment and moisture contents on interactions between lauric acid and starch granules. *J Agric Food Chem*. 2014;62(31):7862-8. <http://doi.org/10.1021/jf501606w>.
54. Shojaei-Aliabadi S, Hosseini H, Mohammadifar MA, Mohammadi A, Ghasemlou M, Ojagh SM, et al. Characterization of antioxidant-antimicrobial  $\kappa$ -carrageenan films containing Satureja hortensis essential oil. *Int J Biol Macromol*. 2013;52:116-24. <http://doi.org/10.1016/j.ijbiomac.2012.08.026>.
55. Barikloo H, Ahmadi E. Shelf life extension of strawberry by temperatures conditioning, chitosan coating, modified atmosphere, and clay and silica nanocomposite packaging. *Sci Hortic*. 2018;240:496-508. <http://doi.org/10.1016/j.scienta.2018.06.012>.
56. Junqueira-Gonçalves MP, Salinas GE, Bruna JE, Niranjan K. An assessment of lactobiopolymer-montmorillonite composites for dip coating applications on fresh strawberries. *J Sci Food Agric*. 2017;97(6):1846-53. <http://doi.org/10.1002/jsfa.7985>.
57. Majdzadeh-Ardakani K, Navarchian AH, Sadeghi F. Optimization of mechanical properties of thermoplastic starch/clay nanocomposites. *Carbohydr Polym*. 2010;79(3):547-54. <http://doi.org/10.1016/j.carbpol.2009.09.001>.
58. Rodrigues R, Patil S, Dhakane-Lad J, Nadanathangam V, Mahapatra A. Effect of green tea extract, ginger essential oil and nanofibrillated cellulose reinforcements in starch films on the keeping quality of strawberries. *J Food Process Preserv*. 2022;46:e15795. <http://doi.org/10.1111/jfpp.16109>.
59. Shankar S, Khodaei D, Lacroix M. Effect of chitosan/essential oils/silver nanoparticles composite films packaging and gamma irradiation on shelf life of strawberries. *Food Hydrocoll*. 2021;117:106750. <http://doi.org/10.1016/j.foodhyd.2021.106750>.

## Data Availability

Full data supporting the findings of this study are available upon request from the corresponding author.